Front. Earth Sci. 2023, 17(1): 337–350
https://doi.org/10.1007/s11707-022-1021-2

RESEARCH ARTICLE

# Characterization of natural fractures in deep-marine shales: a case study of the Wufeng and Longmaxi shale in the Luzhou Block Sichuan Basin, China

**Shasha SUN[1], Saipeng HUANG (✉)[2,3], Enrique GOMEZ-RIVAS[3], Albert GRIERA[4], Bo LIU[2], Lulu XU[5], Yaru WEN[5], Dazhong DONG[1], Zhensheng SHI[1], Yan CHANG[1], Yin XING[6]**

1 PetroChina Research Institute of Petroleum Exploration & Development, Beijing 100083, China
2 Key Laboratory of Continental Shale Hydrocarbon Accumulation and Efficient Development, Ministry of Education, Northeast Petroleum University, Daqing 163318, China
3 Departament de Mineralogia, Petrologia i Geologia Aplicada, Facultat de Ciències de la Terra, Universitat de Barcelona (UB), c/ Martí i Franquès s/n, Barcelona 08028, Spain
4 Departament de Geologia, Universitat Autònoma de Barcelona, Bellaterra 08193, Cerdanyola del Vallès, Spain
5 Hubei Geological Survey, Wuhan 430034, China
6 School of Geography Science and Geomatics Engineering, Suzhou University of Science and Technology, Suzhou 215009, China



**Abstract** Natural fractures are of crucial importance for oil and gas reservoirs, especially for those with ultralow permeability and porosity. The deep-marine shale gas reservoirs of the Wufeng and Longmaxi Formations are typical targets for the study of natural fracture characteristics. Detailed descriptions of full-diameter shale drill core, together with 3D Computed Tomography scans and Formation MicroScanner Image data acquisition, were carried out to characterize microfracture morphology in order to obtain the key parameters of natural fractures in such system. The fracture type, orientation, and their macroscopic and microscopic distribution features are evaluated. The results show that the natural fracture density appears to remarkably decrease in the Wufeng and Longmaxi Formations with increasing the burial depth. Similar trends have been observed for fracture length and aperture. Moreover, the natural fracture density diminishes as the formation thickness increases. There are three main types of natural fractures, which we interpret as (I) mineral-filled fractures (by pyrite and calcite), i.e., veins, (II) those induced by tectonic stress, and (III) those formed by other processes (including diagenetic shrinkage and fluid overpressure). Natural fracture orientations estimated from the studied natural fractures in the Luzhou block are not consistent with the present-day stress field. The difference in tortuosity between horizontally and vertically oriented fractures reveals their morphological complexity. In addition, natural fracture density, host rock formation thickness, average total organic carbon and effective porosity are found to be important factors for evaluating shale gas reservoirs. The study also reveals that the high density of natural fractures is decisive to evaluate the shale gas potential. The results may have significant implications for evaluating favorable exploration areas of shale gas reservoirs and can be applied to optimize hydraulic fracturing for permeability enhancement.

**Keywords** marine shale, natural fracture, filled fracture, tortuosity

Received December 16, 2021; accepted August 1, 2022

E-mail: huangspcugb@hotmail.com

## 1 Introduction

As one of the most important sources of energy, shale gas is becoming a key unconventional resource in China (Zou et al., 2010; Chen et al., 2014; Liu et al., 2022). Reservoirs with multiple natural fracture networks are generally suitable for enhancing their seepage capability because hydraulic fractures can positively influence fracture connectivity (Zhao et al., 2020a). Accordingly, the presence of natural fracture networks in shales is one of the main controlling factors that determine shale gas reservoir productivity (Curtis, 2002; Gale and Holder, 2010; Zeng et al., 2016). The evaluation of natural fractures in hydrocarbon reservoirs has been a hot research topic in recent years (Belfield, 1994; Gale et al., 2007; Ding et al., 2012; Gasparrini et al., 2014; Zhao et al., 2020b; Sun et al.,

2021). Previous studies have shown that the presence of natural fractures in shales contributes to shale gas accumulation and, therefore, promotes gas production (Mullen et al., 2010; Ding et al., 2012). Most natural fractures form owing to tectonic stress, but there are cases in which they can form mostly induced by other processes such as fluid overpressure (Ding et al., 2012). Different types of natural fractures can be found in shales and, in many cases, they can appear in the form of veins, sealed with cement (Gasparrini et al., 2014). Although sealed fractures are not pathways for fluid flow (Laubach, 2003), the vein cement may have different mechanical properties than those of the host rock components, in a way that the vein walls (i.e., interfaces between vein cement and their host rock) can be weaker than the intact host rock and thus may be prone to reactivation (Gale and Holder, 2010; Walton and Mclennan, 2013). The existence of crack-seal veins with localized crack events is an example of how vein walls can be sites of fracture reactivation (Bons et al., 2012). Accordingly, sealed fractures normally play a key role during hydraulic fracturing operations.

Key attributes of natural fractures are their orientation, length, height in the vertical scale, spacing, aperture, fracture-plane strength, and cement (including mineral composition and degree of cementation) (e.g., Huy et al., 2010; Pommer et al., 2012; Wang et al., 2017). Quantifying and predicting natural fracture aperture is of great importance to determine reservoir permeability (Olson et al., 2007; Huy et al., 2010). Many studies have proven that the orientation of natural fractures can be considered as reliable evidence for determining the maximum horizontal principal stress ($\sigma_H$) direction from which these structures formed (Brudy and Zoback, 1999; Paul and Chatterjee, 2011a, 2011b; Liu et al., 2016). However, depending on the tectonic history, fractures may or may not remain aligned with the present-day maximum horizontal stress (Laubach et al., 2004). The evaluation of the reservoir petrophysical properties and the prediction of the propagation direction of hydraulic fractures requires a deep understanding of the *in situ* stress (Huang et al., 2019), and also of the orientation of natural fractures in the reservoir. In addition, the natural fracture tortuosity is another factor that directly controls the available flow paths, which have a significant effect on subsurface fluid flow (Cook et al., 1990). Tsang (1984) showed that the smaller the aperture distribution, the larger the effect of tortuosity.

Fluid inclusions trapped in the vein cements can record the fluid pressure, temperature and fluid composition during fracture crack and seal events (Fall et al., 2012). Therefore, the thermal history of the reservoir can potentially be reconstructed from fluid inclusions in veins. Moreover, the uncertainties of relative and absolute time of fracture formation and sealing can be reduced by combining natural fracture analysis and modern geochemical and geochronological methods (Cruset et al., 2021). Owing to the key role that natural fractures play in oil and gas reservoirs, it is extremely important to understand the mechanisms that determine their formation and evolution, before exploring and developing shale gas plays.

The Longmaxi and Wufeng Formations of the Sichuan Basin (China) contain the most promising hydrocarbon reserves in organic-rich shale in China. Commercial shale gas production has recently been successful in some shale plays. The Luzhou block has the most productive shale gas well, Lu 203, whose daily test output is up to 137.9 $\times$ $10^4$ $m^3$ (Zheng et al., 2019). However, there is a wide variation in production from the different wells of the same play. Although many factors can be responsible for these production differences, a study by Fan et al. (2016) showed that the presence of natural fractures can make differences in production of up to 30%–50% from a single well under the same reservoir conditions. Since recent studies have rarely evaluated the influence of natural fractures in the Luzhou block, here we explore the influence of the natural fracture networks on shale gas production in this area. The analysis of drill core and outcrops is the main way of obtaining information on natural fractures (Abouelresh and Babalola, 2020; Tabatabaei et al., 2021; Cruset et al., 2021). However, natural fractures in outcrops are inevitably affected by exhumation and weathering, sometimes increasing the difficulty of obtaining fracture information that can be representative of subsurface conditions (Mlella et al., 2014). Therefore, a total of five drill core groups (namely LZ1, LZ2, LZ3, LZ4, and LZ5) from the Longmaxi to Wufeng Formations in the Luzhou block were evaluated to characterize the fracture networks in shale. These drill cores were recently obtained from those shale gas wells and are hence unaltered. Moreover, the micro-fractures in the samples were characterized by multiscale 3D CT scanning, which is a commonly used solution to study natural fractures at the microscale (Kim, 2007; Geng et al., 2017; Ranjith et al., 2018; Sang et al., 2019). Accordingly, natural fracture data were obtained and studied at various scales from the microcosmic (approx. 15.68 μm) to the macroscopic (10 cm) scales. The first value corresponds to the 3D CT scan resolution, while the latter is that of the drill core diameter. The research results may have significant applications for the exploration and production of shale gas in this area, and also in similar systems elsewhere.

## 2 Geological setting

The Luzhou block, located in the southern Sichuan Basin, is one of the crucial shale gas production demonstration areas in China. The study area is located in the Fuji syncline, which belongs to the north-western Yanggaosi tectonic group that is part of the high and steep area of the

middle uplift in south-eastern Sichuan. This area is located between the north of the Luoguanshan anticline and the south of the Gufoshan anticline, and its west end is connected with the Shengdenshan field (Fig. 1(a)). Folds are commonly developed in the southern region of the Luzhou block, displaying a NE-SW trend. They are usually distributed in straight or arc-shaped bands, mainly concentrated at the central southern parts of the region,

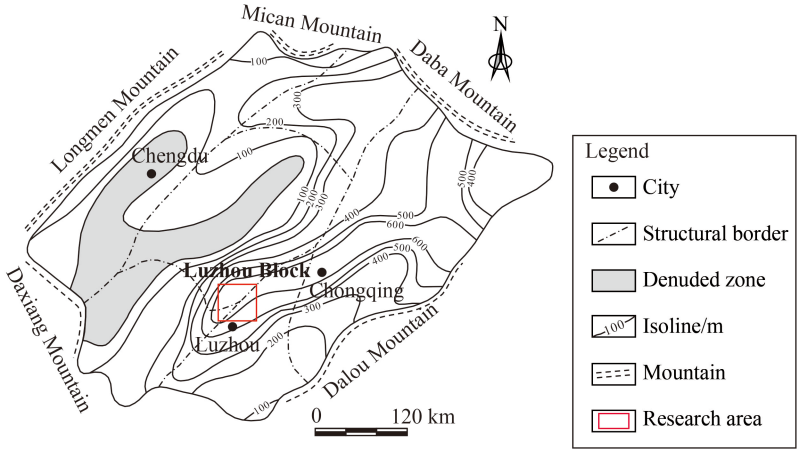


(a)

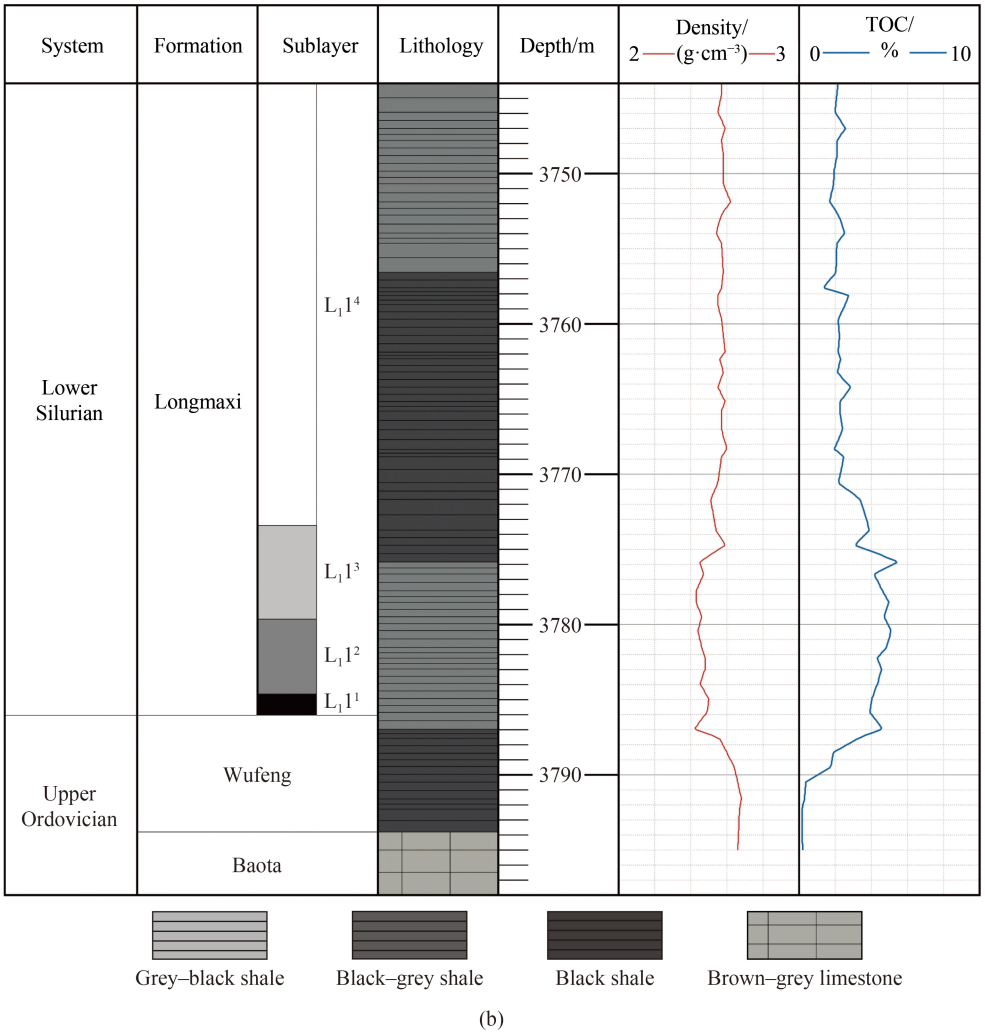


(b)

**Fig. 1** (a) Isopach map of the Longmaxi Formation in the southern Sichuan Basin and location of the Luzhou block (modified from Chen et al. (2011)). (b) Sedimentary and petrophysical logs of the target interval of well LZ4 in the Luzhou block.

and are less developed in its northern part. The synclines are gentle and wide, while the anticline limbs are steeper. Faults are mainly reverse, locally resulting in rock uplift. The study area experienced multiple tectonic evolution events (Feng et al., 2022). The south-eastern Sichuan area was uplifted during the Dongwu movement in the Hercynian orogeny, resulting in the absence of the Upper Silurian, Devonian and Carboniferous units. Moreover, the study area lacks Paleogene and Neogene deposits due to tectonic uplift during the Himalayan period. Thus, the area is mainly dominated by Cambrian and Cretaceous rocks, with occasional Quaternary deposits.

The target reservoirs are located within the Upper Ordovician Wufeng Formation and the Lower Silurian Longmaxi Formation. These two formations mainly consist of black shale, black–gray shale, and gray–black shale. The Longmaxi Formation is about 600 m thick in the Luzhou block (Fig. 1(a)). Organic-rich shales reach 95−140 m in thickness, while high-quality shale gas reservoirs can be up to 40−52 m thick (Chen et al., 2011). The shales of the Longmaxi Formation are divided into two members, $L_1$ and $L_2$. $L_1$ is further divided into two layers, $L_1$1 and $L_1$2. $L_1$1 is the main shale gas producing reservoir (Fig. 1(b)). Furthermore, $L_1$1 is divided into four sublayers of $L_1 1^1$, $L_1 1^2$, $L_1 1^3$, and $L_1 1^4$, and the TOC (Total organic carbon) is much higher in $L_1 1^1$, $L_1 1^2$ and $L_1 1^3$, than in $L_1 1^4$ and in the rocks of the Wufeng Formation.

## 3 Methodology

### 3.1 Observation and description of natural fractures

Natural fractures are complex in shales, and their shape is usually irregular (Gale et al., 2014). Normally, the fracture length, height along the vertical scale, and aperture are the basic assessment parameters when analyzing drill core (Fig. 2(a)). Furthermore, fracture spacing is another important factor for the evaluation of fracture density (Fig. 2(b)). In this study, full-diameter shale cores are observed and described in detail. It is difficult to predict the actual size of natural fractures merely from drill cores, given that the diameter of the drill core is only 10 cm, whereas many fractures may run through the core resulting in censoring bias (Zeeb et al., 2013). Moreover, it is always problematic to characterize the length scale from fracture logs. Therefore, the maximum natural fracture lengths in this type of description depend on the well orientation. Drill cores were newly collected in shales of the Luzhou block, and a total of five groups of cores from each shale gas well were observed. They correspond to the Longmaxi and Wufeng Formations. A total of 247 m of full-diameter shale core was observed, and the description accuracy of the natural fractures found reaches the millimeter scale. Essential data, including the type of fracture, their length, aperture, density, and dip were recorded, together with their filling. Moreover, fractures were divided into three types according to their aperture: large (larger than 5 mm), intermediate (between 1 to 5 mm), and small (less than 1 mm). Furthermore, we divided natural fractures from drill cores according to their orientation in vertical (with dips greater than 80°), oblique (with dips ranging between 10° and 80°), and horizontal fractures (with dips lower than 10°).

In addition, the FMI (Formation MicroScanner Image) data of formation resistivity were used to identify the natural fractures and determine their orientation. The total thickness of FMI interpreted data was 74 m for the LZ1 well, 52 m for LZ2, 45 m for LZ3, and 51 m for LZ4. The threshold segmentation of the image was defined through the processing of gray band of the original FMI data. Fracture orientation parameters like dip direction and dip were obtained by using the Hough transformation. The fracture data were summarized for every 5 m, and then summed up together for every well. Interpretation of FMI data allowed an accuracy at least 5 mm. The *in situ* stress orientation data around the Luzhou block was obtained from the World Stress Map Database Release 2016 (Heidbach et al., 2016a, 2016b, 2018) with the aim of analyzing differences between the present-day stress field and that inferred from natural fracture orientations to better understand potential fracture formation time.

### 3.2 Evaluation of shale gas well considering natural fractures

A wide range of reservoir properties like depth, reservoir thickness, TOC, vitrinite reflectance, permeability, gas

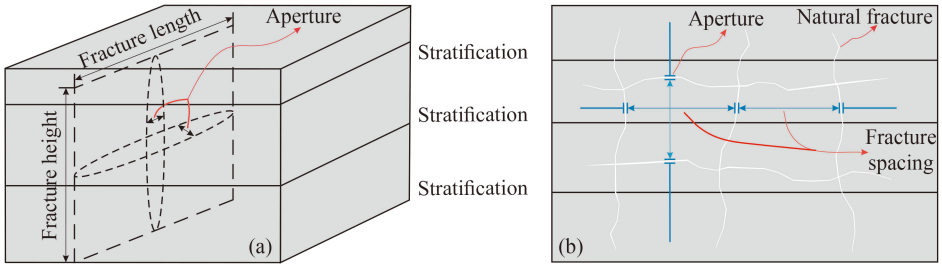


**Fig. 2** (a) Sketch of a natural fracture in shale. (b) Diagram showing some of the key parameters used to describe fractures in this study.

content, reservoir pressure etc. can be used to predict shale-gas production (Curtis, 2002). For example, Hill and Nelson (2000) proposed thermal maturity, gas in place, TOC, reservoir thickness, and proportion of sorbed gas as key parameters to predict gas-shale and geochemical properties of different petroleum systems. A similar evaluation method was applied in this study. After the description of the natural fractures in shale, the wells were evaluated according to four parameters from the target formation: density of natural fractures, formation thickness, average TOC, and effective porosity. Among these data, the average TOC, and the effective porosity are quantified from the well logs, while the fracture density results from the detailed description of the cores.

### 3.3 Multiscale 3D CT scans of fractures in shale

In addition to the macroscopic observations of natural fractures from drill cores, their microcosmic characteristics were also analyzed using multiscale 3D CT scans. The core from well LZ4 in the sublayers of $L_1 1^3$ with the depth of 3776.98−3777.11 m was scanned at multiple scales to visualize the natural fractures. For the target core with a diameter of 25 mm, three sections in the horizontal and vertical directions were selected to analyze fracture tortuosity. The scanning resolution reached 15.68 μm, which is high enough to characterize natural fractures. A total of 3000 slices were obtained from CT scanning, and then analyzed to display the fracture morphology using the program Avizo. Tortuosity ($\alpha$) is considered a useful parameter to describe the fracture roughness on a cross-section, which can effectively reflect the geometrical complexity of natural fractures:

$$\alpha = \frac{l}{L}, \tag{1}$$

where $l$ is the real length of the natural fracture and $L$ is the straight-line distance between the two fracture endpoints.

## 4 Results

### 4.1 Macroscopic distribution characteristics of natural fractures

The distribution of natural fractures along the vertical direction of the five wells is displayed in Fig. 3. The maximum frequencies of natural fractures are mainly observed in the lower part of the Longmaxi and Wufeng Formations. They are marked in Fig. 3 by the red rectangles, which correspond to the major shale gas production reservoirs in the Luzhou block. The fracture densities for wells LZ1, LZ2, LZ3, LZ4, and LZ5 are 6.94/m, 6.33/m, 3.72/m, 9.1/m, and 4.28/m, respectively. In general, fracture density remarkably decreases with the increasing burial depth of the shale gas reservoir (Fig. 4).

By analyzing the observed data from the shale gas well LZ1, the natural fracture occurrence shows a gradual increasing trend in the Lower Silurian Longmaxi Formation, while the number of fractures rapidly decreases during the transition to the Upper Ordovician Wufeng Formation and then continuously decreases in

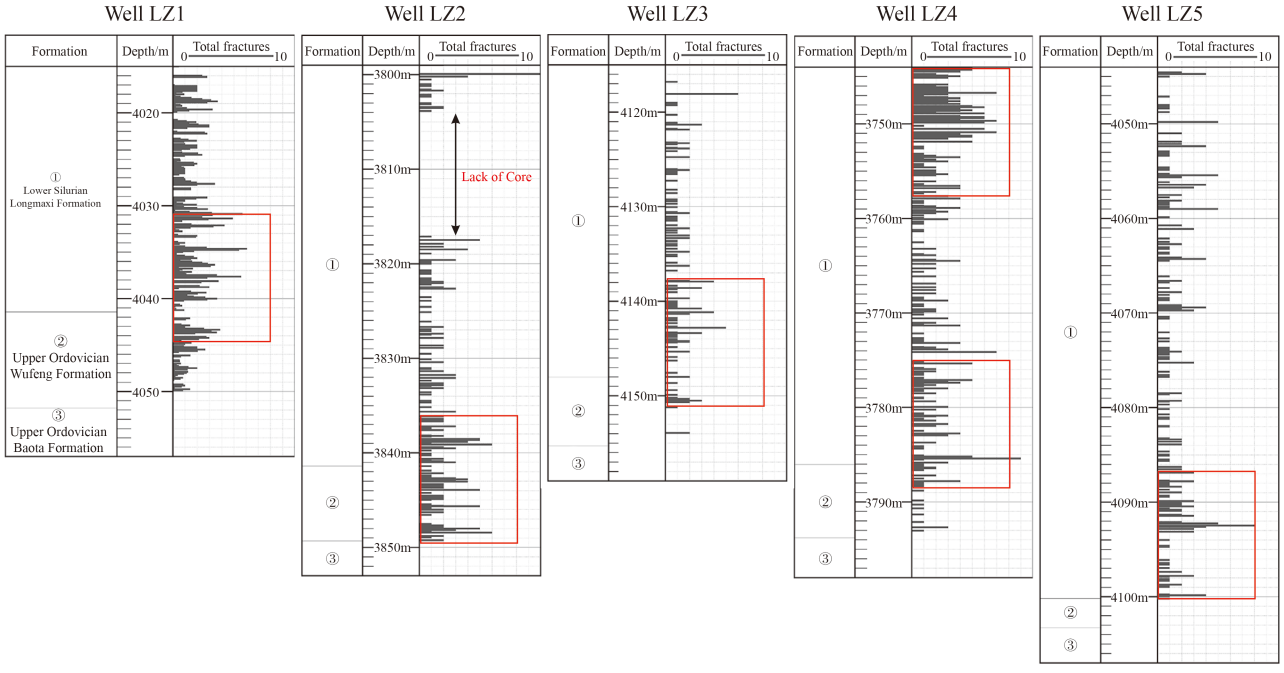


**Fig. 3** The total number of natural fractures in the vertical dimension for wells LZ1 to LZ5. The red rectangles indicate the part with a higher fracture density.

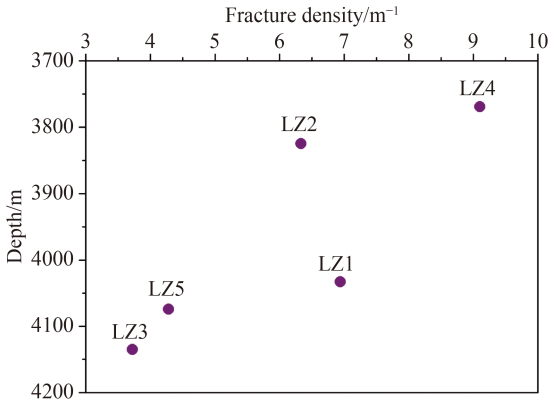


**Fig. 4** Fracture density vs. reservoir depth in the Luzhou block.

the Wufeng Formation (Fig. 5). The fracture aperture range between 1 and 5 mm is dominant, and horizontal fractures constitute the majority of the natural fractures analyzed. Moreover, a high TOC content appears in the lower part of the Longmaxi Formation, and fracture density shows a similar trend to that of the TOC.

### 4.2 Natural fracture type and its physical characteristics

Natural fractures observed in the full diameter shale cores have been divided into three types in this study. Type I fractures are defined as those filled with cement (i.e., veins). Type II fractures are those that show evidence of slip along fault walls, while Type III fractures include bedding-parallel fractures and those fractures without slip evidence. The minerals filling type I fractures (i.e., veins) are mostly calcite and pyrite (Fig. 6). Although quartz-filled fractures are also commonly found in the Wufeng and Longmaxi Formations (Nie et al., 2020; Qiu et al. 2020), only a small proportion of the fractures appear cemented by quartz in our studied well intervals. Calcite-filling fractures often occur in the form of fracture networks, and sometimes calcite also fills bedding-parallel fractures on a small scale of less than 0.5 mm (Fig. 6(a)). In addition, since calcite is a brittle mineral that can easily get cracked, many small fractures can be found within the calcite veins (Fig. 6(b)). The fracture network filled with calcite always shows a heterogeneous distribution (Fig. 6(c)). Overall, secondary fractures are more likely to be generated within the shale, where calcite veins are developed. Fractures filled with pyrite always appear in the form of bands (Figs. 6(d) and 6(e)), and, as it happens to calcite veins, it is common that refracturing affects pyrite veins. Moreover, features indicating fracture dissolution can also be observed (Fig. 6(e)). Furthermore, nodules of pyrite are spheroidal, commonly found in shale, and calcite rims can occasionally be seen at the edge of the pyrite nodules (Fig. 6(f)). Filled fractures (i.e., veins) can form from

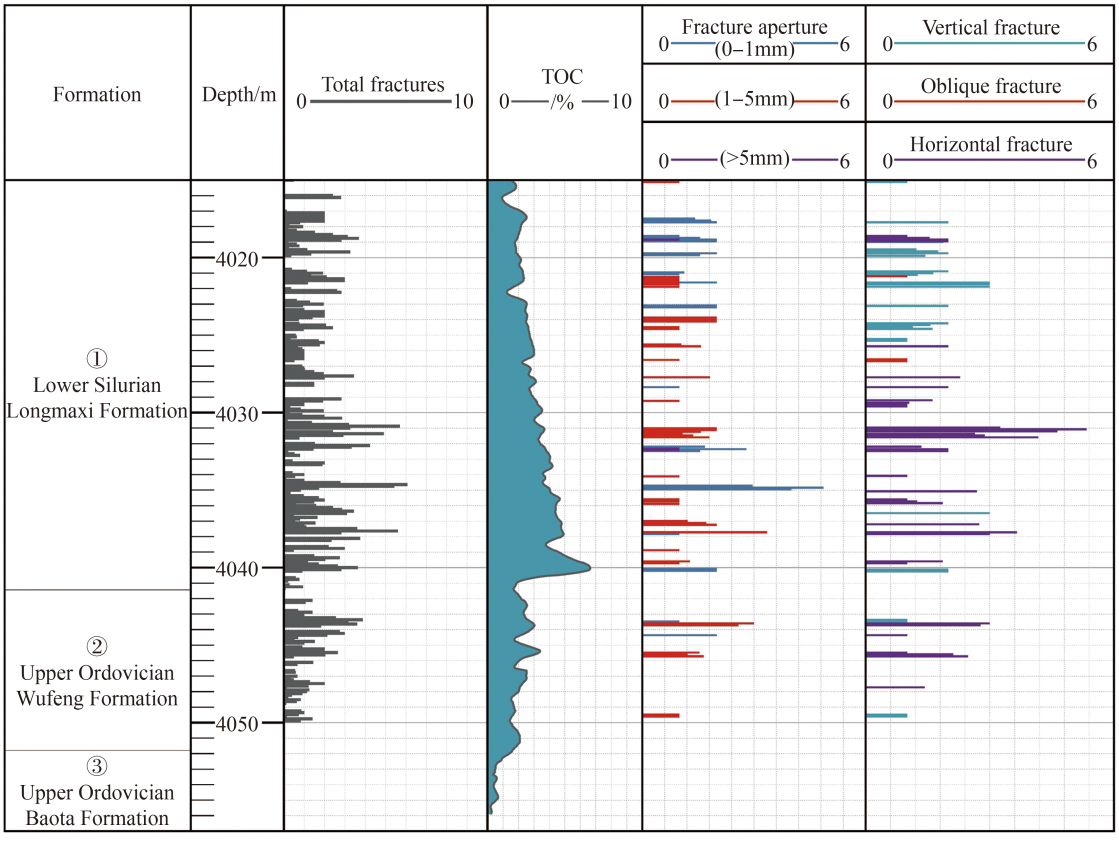


**Fig. 5** Distribution of natural fractures in well LZ1.

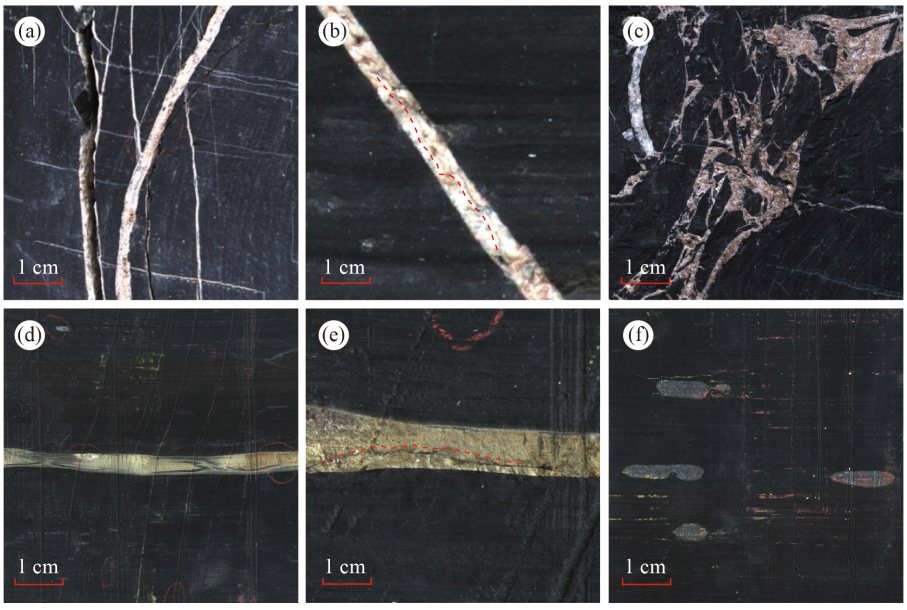


**Fig. 6** (a−e) Example of Type I natural fractures (i.e., veins). (a) Fracture filled with calcite vein from LZ1 well (3935.21−3935.53 m), (b) fracture formed in calcite vein from LZ1 well (3951.07−3951.22 m), (c) fracture network filled with calcite veins from LZ1 well (3946.48−3946.69 m), (d) fracture with pyrite filled from LZ2 well (3799.55−3799.86 m), (e) fracture formed in pyrite vein from LZ2 well (3798.55−3798.80 m), (f) pyrite nodules from LZ2 well (3795.10−3795.42 m).

type II and III fractures.

Type II fractures are interpreted as those formed by the action of tectonic stress (the so-called "structural fractures" by Zhang et al. (2019)). In general, they show evidence of relative displacement between fault walls. For example, Fig. 7(a) shows two fractures all go through the full-diameter core, and the angle of the crossing fracture is close to 75°. Some of these fractures are irregularly shaped (Fig. 7(b)), and mineral precipitates are barely found sealing them. A complex fracture network with parallel fractures is observed in Fig. 7(c), without cement filling. An oblique fracture with normal dip slip displacement can be found with cement-filled (Fig. 7(d)). The Type II fractures are generally observed in our study.

The bedding-parallel fractures of Fig. 8(a) are easy to recognize with the naked eye, normally have a characteristic banding distribution along the plane, and are actually parallel to each other, but barely found filled

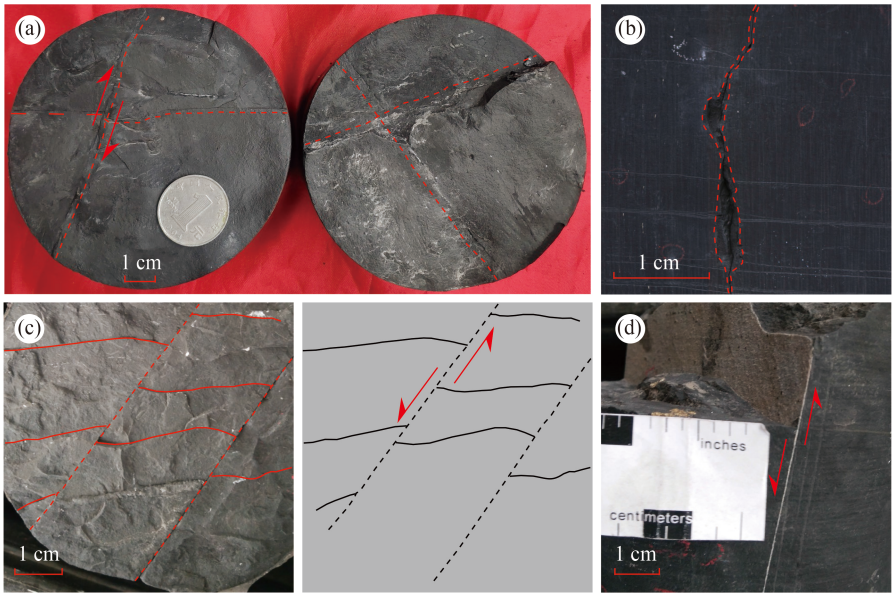


**Fig. 7** Example of type II fractures. (a) Conjugate strike-slip faults from LZ2 well (3842.70−3842.90 m depth), (b) from LZ1 well (3968.46−3968.64 m), (c) parallel strike-slip faults from LZ1 well (4034.47−4034.66 m), (d) sub-vertical normal fault from LZ1 well (4022.20−4022.37 m).

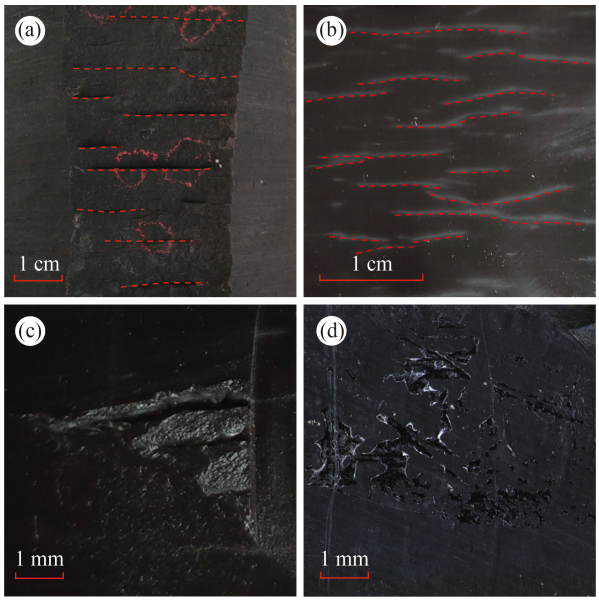


**Fig. 8** Several examples of typical fractures formed by other processes than tectonic stress (so-called non-structural by Zhang et al. (2019)). (a) Bedding-parallel fractures from LZ1 well (4035.38–4035.55 m), (b) bedding-parallel fractures from LZ4 well (3782.75–3782.95 m), (c) induced fracture from LZ4 well (3772.17–3772.32 m) and (d) induced fracture from LZ1 well (3983.72–3983.99 m).

with mineral precipitates. An example of a bedding-parallel fracture is displayed in Fig. 8(b). It is short and is not continuous compared to the fracture of Fig. 8(a). These fractures are hard to identify unless the rock surface is wiped with a wet towel in which case, they become visible because they absorb water. The further action of *in situ* stress in shale can result in heterogeneous deformation at the small scale, thus leading to bending and discontinuity of bedding-parallel fractures. These fractures, which present irregular shapes and small sizes, are not continuously observed in shale (Fig. 8(c)). They are irregularly shaped and are can be connected together by a large number of small filled vugs at different depths (Fig. 8(d)). Consequently, these fractures are likely to disappear by late compaction or mineral filling.

### 4.3 Natural fracture parameters

Figure 9 presents information on fracture parameters from wells LZ1, LZ2, LZ3, LZ4, and LZ5. Apparently, horizontal (bedding-parallel) fractures are the most abundant (Fig. 9(a)). The apertures of natural fractures are mostly lower than 5 mm. Fractures from LZ2 and LZ3 mainly have apertures ranging between 1 mm and 5 mm, and the majority of them are lower than 1 mm in the LZ1, LZ4, and LZ5 wells (Fig. 9(b)). Although the cements filling the fractures correspond to different minerals, pyrite and calcite are the most visible cements and the easiest to recognize. Pyrite is the most widely distributed mineral fill (Fig. 9(c)), and sometimes appears

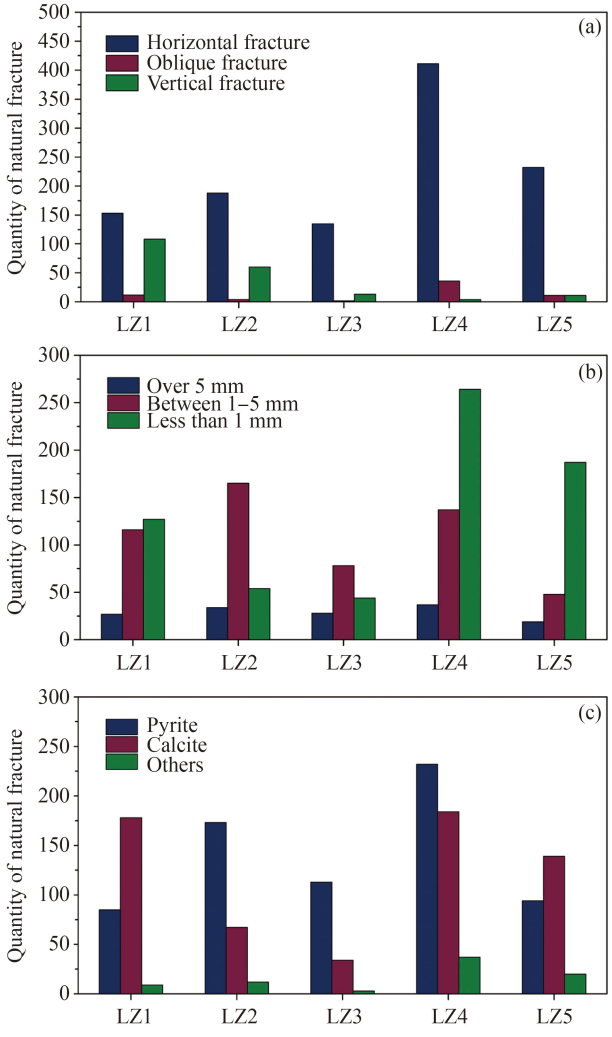


**Fig. 9** Frequency of fracture (a) dip type, (b) aperture, and (c) filled cement.

in the form of bands and nodules.

### 4.4 Burial depth vs. fracture length and aperture

The length and aperture of natural fractures in LZ4 are displayed in Fig. 10. The natural fractures in LZ4 are mainly divided into horizontal and oblique fractures. The relationship between burial depth and fracture aperture and length are analyzed. The results show that the apertures have a decreasing trend with the increasing depth (Fig. 10(a)). The length of natural fractures also presents a similar trend (Fig. 10(b)). The range of apertures of oblique fractures ranges between 0.2 mm and 1.8 mm, while the apertures of horizontal fractures vary between 0.2 mm and 0.5 mm. Apparently, the apertures of oblique fractures are larger than those of horizontal fractures. However, their lengths are similar in the core size. Furthermore, it seems that the length of horizontal fractures decreases more rapidly than that of the oblique fracture as the formation depth increases.

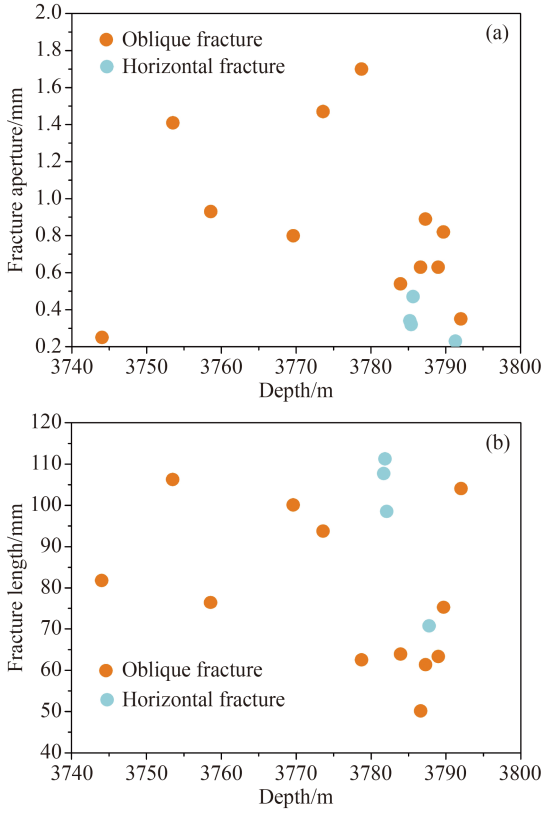


**Fig. 10** (a) Burial depth vs. natural fracture aperture. (b) Burial depth vs. natural fracture length.

## 4.5 Fracture density in the Wufeng and Longmaxi Formations

The fracture densities were collected from four shale gas wells for each formation. The thickness of the Wufeng Formation ranges between 3 and 10 m, and falls between 30 and 65 m for the Longmaxi Formation in the Luzhou block. The results show that the fracture density in the Wufeng Formation decreases rapidly as the formation thickness slightly increases, but decreases more slowly in the Longmaxi Formation (Fig. 11).

## 4.6 Natural fracture orientations estimated from FMI

The fracture dip direction and dip of natural fractures in the Longmaxi and Wufeng Formations obtained from FMI logs are displayed in Fig. 12. The dip directions of natural fractures in LZ1 are relatively consistent and commonly range between NW 40° and 60°. The main orientation is approximately NW 50°, and the dip ranges between 20° and 25° (Figs. 12(a) and 12(b)). Fractures from LZ2 and LZ3 have small dips (< 10°), indicating that that low-angle and horizontal fractures are both well developed (Figs. 12(c) and 12(e)). It is quite unique that fracture orientations in LZ2 are dominated by more than one direction (Fig. 12d). The dominant fracture dip for LZ4 is 35° (Fig. 12(g)). Similarly, the dominant dip directions of LZ3 and LZ4 are NW 85° and NW 70°, respectively. Therefore, both have approximately N-S to NNE-SSW strikes (Figs. 12(f) and 12(h)).

## 4.7 Natural fracture microscopic features

Results from 3D CT scans are shown in Fig. 13. Three

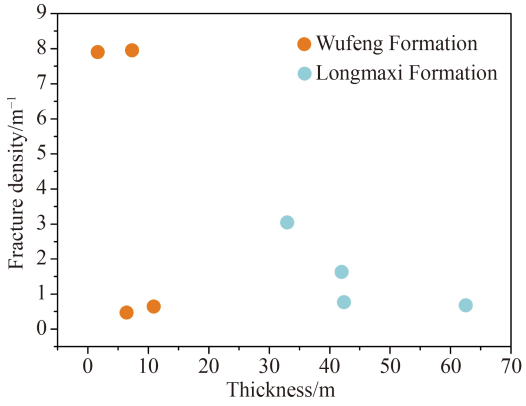


**Fig. 11** Formation thickness vs. fracture density.

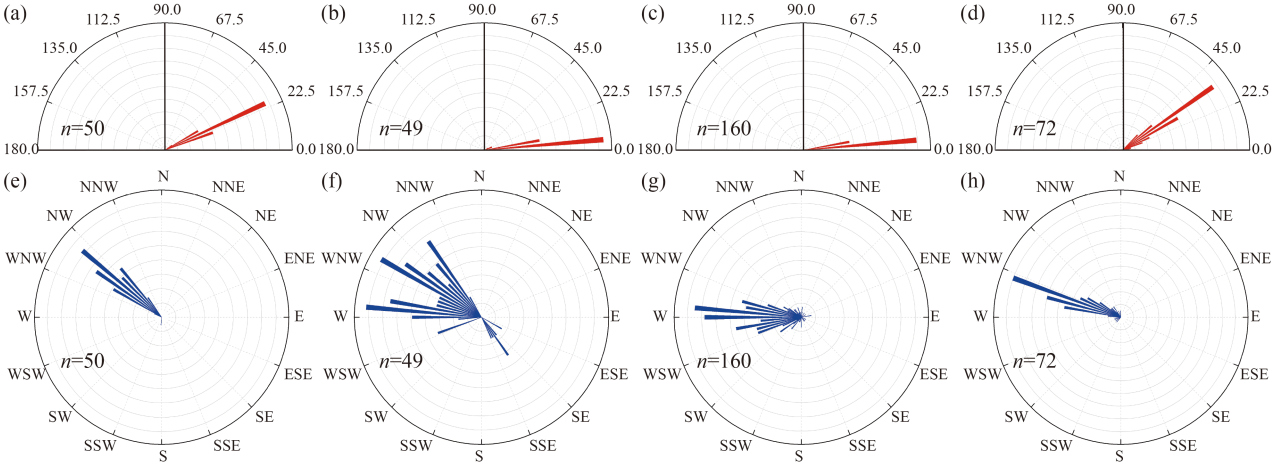


**Fig. 12** (a–h) Dip (red) and dip direction (blue) of natural fractures from LZ1, LZ2, LZ3, and LZ4 wells, respectively.

horizontal and vertical sections of the drill core were used to analyze microscopic fractures (Fig. 13(a)). As shown in Fig. 13(b), some zones with a special concentration of fine pyrites are observed (pyritization zones). Similarly, similar zones can also be found in the vertical sections (Fig. 13(c)). At a resolution of 15.68 μm (i.e., that of the CT scan), almost none of the natural fractures appear filled with cement. However, pyritization zones are commonly found. Moreover, natural fractures are nearly spread along pyritization zones. The orientations of natural fractures in both the horizontal and vertical directions of the cores are summarized in Figs. 13(d) and 13(e). The NF length-L1 and NFS length-L2 in Fig. 13 are the natural fracture original lengths and the natural fracture section length, respectively. The Tortuosity ($\alpha$) values of natural fractures have been calculated with Eq. (1). The distribution of tortuosities in the horizontal and vertical sections is displayed in Fig. 14. Values span approx. from 1 to 1.10.

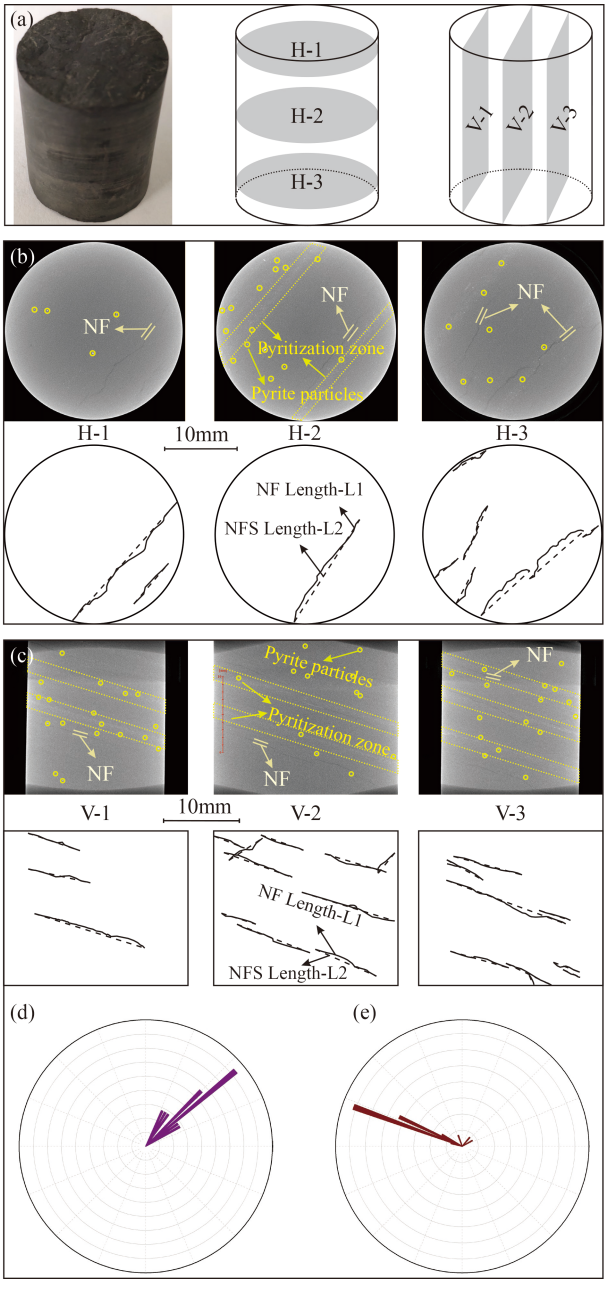


**Fig. 13** (a–c) 3D CT scans in the horizontal and vertical directions with a diameter of 25 mm. The digitalised fractures (black lines) and envelopes (dashed lines) are indicated. (d–e) Summary of the natural fracture orientation, (d) fracture dip directions and (e) dips respect to bedding.

## 5 Discussion

### 5.1 Distribution of natural fractures in full-diameter drill cores

Although the total number of natural fractures in the vertical dimension for each well is different (Fig. 3), the results show that the more productive shale gas formation is consistent with depth levels in which fractures are relatively well developed. This demonstrates that the presence of natural fractures can be a potential factor in order to select the most favorable shale gas plays.

Some authors classify natural fractures in shale into two main categories: structural fractures and non-structural fractures (Zhang et al., 2019). Here we have decided to classify fractures in three types. Type I fractures are those mineralized with cement (mostly with calcite or pyrite). Since calcite veins can easily get cracked, these types of fractures can help to connect fracture networks during hydraulic fracturing. Type II fractures are interpreted as formed as a result of the action of tectonic stress and are commonly observed in the Longmaxi Formation. For example, the evidence of conjugate shear fractures (Fig. 7(a)) or slip displacement along fault walls (e.g., normal and strike-slip components) (Figs. 7(c) and 7(d)) allows us to interpret these structures as produced by tectonic processes. Another typical fracture formed under strike-slip (Fig. 7(c)) has associated fracture networks, which can enhance the connection of pores of the shale matrix. Faults with normal offsets and partial filling can be found (Fig. 7(d)). This type of fracture often presents large dips in the studied cores. Type II fractures would correspond to the “structural fractures” of Zhang et al. (2019) and are normally larger in width size than that of

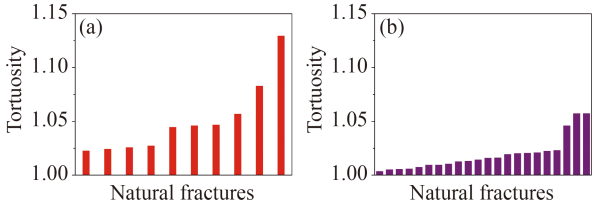


**Fig. 14** Tortuosity of the natural fractures. (a) horizontal direction, (b) vertical direction.

type I and III. Type III fractures are typical small in length, irregular, and without evident slip components, as for example the fractures displayed in Fig. 8(c). They are interpreted as the non-structural fractures of Zhang et al. (2019), and most of them are probably induced by fluid overpressure and shrinkage, etc. Such overpressure can result from the organic matter hydrocarbon discharge in shale. The difference in total filled cement of the five wells in Fig. 9(c) indicates that shale is highly heterogeneous, so a typical shale gas well cannot be completely representative of the shale properties of the entire research area. In addition, the fracture density relationship with reservoir thickness as shown in Fig. 11 reveals that the target reservoir thickness can be used as one of the factors to predict fracture density tendency in the absence of fracture data in a new research area.

### 5.2 Orientation of natural fractures versus *in situ* stress field

The summary of all the FMI logs shows that the natural fracture dips are mostly lower than 22.5°, and the dominating dip is approximately in the range of 5°−10°. This reveals that horizontal fractures are the most common type in the Luzhou block (Fig. 15(a)). Although the dominant fracture dip directions of LZ2 are very variable, the main orientations from the whole block are NW 70°−75° and NW 55°. The similarity in fracture orientations from the LZ1 and LZ4 wells indicates that they were probably formed by a single tectonic event (Figs. 12(a), 12(b), 12(g), and 12(h)).

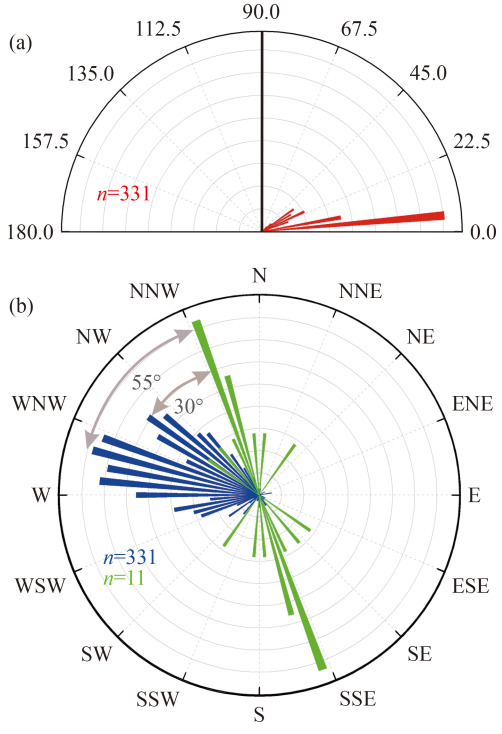


**Fig. 15** Natural fracture (a) dips (red) and (b) dip directions (blue) compared to present-day maximum horizontal principal stress ($\sigma_H$) orientations (green) for the Luzhou block.

An important question is if the observed natural fractures reflect the current *in situ* stress field in the reservoir or not. The World Stress Map Database Release 2016 (Heidbach et al., 2016a, 2016b, 2018) collects stress field data and provides a way to infer the current regional orientation of maximum horizontal principal stress ($\sigma_H$). Most of the data were obtained from earthquake focal mechanisms, borehole breakouts, hydraulic fracturing measurements, fault-slip data, drilling-induced tensile fractures of the borehole wall and borehole slotter, etc., which are all effective ways to obtain the stress direction. A total of data from 11 wells around the Luzhou block were chosen from the World Stress Map Database (Table 1), in order to compare $\sigma_H$ orientations with the ones obtained from the fracture networks analyzed from wells. The depth of these wells ranges between 3 and 4 km, and these values are close to those of the Luzhou block target formations. The dominant present-day $\sigma_H$ orientation is approximately NW 22°. Our data on fracture dip directions show two dominant maxima (NW 70°−75° and NW 55°), making an angle of 30° and 55° with respect to the present-day direction of $\sigma_H$ (Fig. 15(b)). Tensile fractures form parallel to $\sigma_H$, while conjugate shear fractures form at symmetric angles with respect to $\sigma_H$, depending on the frictional coefficient of rocks (e.g., Fossen, 2010). Our data do not match the $\sigma_H$ orientation obtained from the World Stress Map, independent of if natural fractures are interpreted as tensile or shear fractures. Therefore, it can be concluded that these fractures did not form according to the present-day stress field. In addition, since hydraulic fracture propagation is commonly influenced by the current direction of $\sigma_H$ (Lakirouhani et al., 2016; Zhang et al., 2018), it is necessary to adjust the hydraulic fracturing measures to induce more fracture networks, considering both the directions of natural fractures and the present-day $\sigma_H$.

**Table 1** Detailed information of the orientation of the present-day maximum horizontal principal stress ($\sigma_H$) near the Luzhou block. Data have been taken from Heidbach et al. (2016a, 2016b).

| Well | $\sigma_H$ orientation | Method used to obtain the data | Depth/km |
|---|---|---|---|
| 1 | 160° | Borehole breakouts | 3.03 |
| 2 | 160° | Borehole breakouts | 2.58 |
| 3 | 140° | Earthquake focal mechanisms | 8 |
| 4 | 160° | Borehole breakouts | 2.95 |
| 5 | 175° | Borehole breakouts | 3.15 |
| 6 | 5° | Borehole breakouts | 3.2 |
| 7 | 125° | Borehole breakouts | 3.12 |
| 8 | 38° | Borehole breakouts | 4.3 |
| 9 | 155° | Borehole breakouts | 4.33 |
| 10 | 165° | Borehole breakouts | 2.7 |
| 11 | 165° | Borehole breakouts | 4.4 |

### 5.3 Comprehensive evaluation of the shale gas wells

Figure 16 shows that wells LZ1, LZ3, LZ4, and LZ5 have no significant difference in the average TOC and effective porosity. Therefore, these wells from the Luzhou block all have similar reservoir physical parameters. In addition, due to the obvious difference in the natural fracture density and formation thickness, they can be used as important parameters to evaluate shale gas wells. A variety of factors, like natural fracture density, formation thickness, effective porosity, average TOC, average permeability, and gas content of the reservoir should be taken into account to estimate the quality of a well. However, the permeability and gas content data are incomplete for the four wells, and therefore we cannot discuss them in detail. The well LZ4 is recognized as that with the greatest potential for shale gas well according to the available data.

### 5.4 Natural fracture representation and tortuosity

Sample from the drill core corresponding to well LZ4 was chosen because this well shows the highest potential for shale gas production according to the well comprehensive evaluation of Section 5.3. Figures 13(d) and 13(e) show that, although natural fractures are discontinuous, their extension directions are relatively consistent. Apparently, the $\alpha$ value in the horizontal direction is much larger than that in the vertical direction (Fig. 14). In fact, although the $\alpha$ values are obtained from two directions that are perpendicular to each other, $\alpha$ manifestly indicates the same group of fractures in the core. The $\alpha$ difference between the horizontal and vertical directions demonstrates the geometrical complexity of natural fractures. Moreover, many studies have shown an inverse correlation between tortuosity and permeability (Wang et al., 2005; Zhu and Wong, 1996). Accordingly, the role of tortuosity and its relation with connectivity for the influence of permeability needs further investigation (Cai et al., 2019).

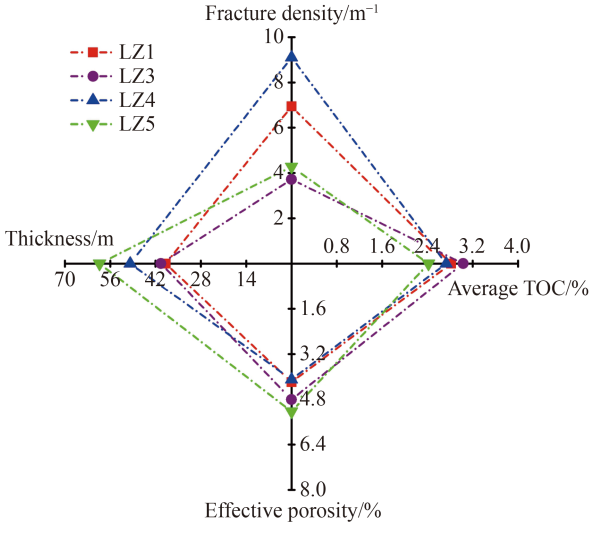


**Fig. 16** Spider diagram evaluating the main four parameters for predictive shale gas obtained from the four studied wells.

## 6 Conclusions

This study presents a characterization and evaluation of natural fractures of the Wufeng and Longmaxi Formation shales in the Luzhou Block, Sichuan Basin, based on observations and descriptions of full-diameter shale cores, FMI logs and 3D CT scans. The fracture types, their orientation, and macroscopic and microscopic distribution features are analyzed and discussed. Tortuosity was also considered for the evaluation of the natural fracture complexity. The results may have significant implications for evaluating favorable exploration areas of shale gas reservoirs. The following conclusions were obtained.

1) The natural fracture density remarkably appears to fall with increasing burial depth in the Wufeng and Longmaxi Formations. Similar trends are observed for fracture length and aperture. Moreover, the natural fracture density diminishes as the thickness of these formations increases.

2) Natural fractures can mainly be classified into three distinct types. The first type is filled fractures (veins). The other two types correspond to fractures dominantly formed as a consequence of tectonic stress or by other processes such as fluid overpressure and diagenetic shrinkage.

3) Natural fracture orientations in the Luzhou block are not consistent with the present-day stress field.

4) Although natural fractures are discontinuous at the microscale, their extension directions are relatively consistent and often occur in clusters. The tortuosity difference between the horizontal and vertical direction manifestly indicates their geometrical complexity of these natural fractures.

**Acknowledgments** The project is funded by the National Natural Science Foundation of China (Grant No. 42202155), China Postdoctoral Science Foundation (No. 2021MD703807), Major Special Project of the Ministry of Science and Technology of PetroChina (Nos. 2022DJ8004 and 2021DJ1901), Heilongjiang Postdoctoral Foundation (No. LBH-Z20121), Natural Science Foundation of Hubei Province Project (No. 2020CFB501) and The Scientific Research Project of Department of Natural Resources of Hubei Province (No. ZRZY2020KJ10). The authors gratefully acknowledge financial support from the China Scholarship Council (No. 202008230018). EGR acknowledges funding by the Spanish Ministry of Science and Innovation (MCIN)/State Research Agency of Spain (AEI)/European Regional Development Fund (ERDF)/10.13039/501100011033 for the "Ramón y Cajal" fellowship RYC2018-026335-I and research projects PGC2018-093903-B-C22 and PID2020-118999GB-I00.

## References

Abouelresh M O, Babalola L O (2020). 2D spatial analysis of the

natural fractures in the organic-rich Qusaiba Shale outcrop, NW Saudi Arabia. J Petrol Sci Eng, 186: 106780

Belfield W C (1994). Multifractal characteristics of natural fracture apertures. Geophys Res Lett, 21(24): 2641–2644

Bons P D, Elburg M A, Gomez-Rivas E (2012). A review of the formation of tectonic veins and their microstructures. J Struct Geol, 43: 33–62

Brudy M, Zoback M D (1999). Drilling-induced tensile wall-fractures: implications for determination of *in-situ* stress orientation and magnitude. Int J Rock Mech Min Sci, 36(2): 191–215

Cai J C, Zhang Z E, Wei W, Guo D M, Li S, Zhao P Q (2019). The critical factors for permeability-formation factor relation in reservoir rocks: pore-throat ratio, tortuosity and connectivity. Energy, 188: 116051

Chen S B, Zhu Y M, Qin Y, Wang H Y, Liu H L, Fang J H (2014). Reservoir evaluation of the Lower Silurian Longmaxi Formation shale gas in the southern Sichuan Basin of China. Mar Pet Geol, 57: 619–630

Chen S B, Zhu Y M, Wang H Y, Liu H L, Wei W, Fang J H (2011). Shale gas reservoir characterisation: a typical case in the southern Sichuan Basin of China. Energy, 36(11): 6609–6616

Cook A M, Myer L R, Cook N G W, Doyle F M (1990). The effects of tortuosity on flow through a natural fracture. In: Rock Mechanics Contributions and Challenges: Proceedings of the 31st U S Symposium. New York: CRC Press

Cruset D, Vergés J, Benedicto A, Gomez-Rivas E, Cantarero I, John C M, Travé A (2021). Multiple fluid flow events from salt-related rifting to basin inversion (Upper Pedraforca thrust sheet, SE Pyrenees). Basin Res, 33(6): 3102–3136

Curtis J B (2002). Fractured shale-gas systems. AAPG Bull, 86(11): 1921–1938

Ding W L, Li C, Li C Y, Xu C C, Jiu K, Zeng W T, Wu L M (2012). Fracture development in shale and its relationship to gas accumulation. Geosci Front, 3(1): 97–105

Fall A, Eichhubl P, Laubach S E, Bodnar R J (2012). Timing and duration of gas charge-driven fracturing in tight-gas sandstone reservoirs based on fluid inclusion observations: Piceance Basin, Colorado. In: AGU Fall Meeting

Feng Q Q, Qiu N S, Borjigin T, Wu H, Zhang J T, Shen B J, Wang J S (2022). Tectonic evolution revealed by thermo-kinematic and its effect on shale gas preservation. Energy, 240: 122781

Fan J M, Qu X F, Wang C, Lei Q, Cheng L, Yang Z (2016). Natural fracture distribution and a new method predicting effective fractures in tight oil reservoirs of Ordos Basin, NW China. Pet Explor Dev, 43(5): 806–814

Fossen H (2010). Structural Geology. London: Cambridge University Press

Gale J F W, Holder J (2010). Natural fractures in some US Shales and their importance for gas production. In: Petroleum Geology Conference series. London: Geological Society: 1131–1140

Gale J F W, Laubach S E, Olson J E, Eichhubl P, Fall A (2014). Natural fractures in shale: a review and new observations. AAPG Bull, 98(11): 2165–2216

Gale J F W, Reed R M, Holder J (2007). Natural fractures in the Barnett shale and their importance for hydraulic fracture treatments. AAPG Bull, 91(4): 603–622

Gasparrini M, Sassi W, Gale J F W (2014). Natural sealed fractures in mudrocks: a case study tied to burial history from the Barnett Shale, Fort Worth Basin, Texas, USA. Mar Pet Geol, 55: 122–141

Geng Y, Liang W, Liu J, Cao M, Kang Z (2017). Evolution of pore and fracture structure of oil shale under high temperature and high pressure. Energy Fuels, 31(10): 10404–10413

Heidbach O, Rajabi M, Cui X F, Fuchs K, Müller B, Reinecker J, Reiter K, Tingay M, Wenzel F, Xie F R, Ziegler M O, Zoback M L, Zoback M (2018). The World Stress Map database release 2016: Crustal stress pattern across scales. Tectonophysics, 744: 484–498

Heidbach O, Rajabi M, Reiter K, Ziegler M (2016a). World Stress Map 2016, GFZ Data Services

Heidbach O, Rajabi M, Reiter K, Ziegler M (2016b). World Stress Map Database Release 2016. GFZ Data Services

Hill D G, Nelson C R (2000). Gas productive fractured shales: an overview and update. Gas TIPS, 6(2): 4–13

Huang S P, Liu D M, Cai Y D, Gan Q (2019). *In situ* stress distribution and its impact on CBM reservoir properties in the Zhengzhuang area, Southern Qinshui Basin, North China. J Nat Gas Sci Eng, 61: 83–96

Huy P Q, Sasaki K, Sugai Y, Ichikawa S (2010). Carbon dioxide gas permeability of coal core samples and estimation of fracture aperture width. Int J Coal Geol, 83(1): 1–10

Kim T H (2007). Fracture characterization and estimation of fracture porosity of naturally fractured reservoirs with no matrix porosity using stochastic fractal models. Dissertation for the doctoral Degree. College Station: Texas A&M University

Lakirouhani A, Detournay E, Bunger A P (2016). A reassessment of in-situ stress determination by hydraulic fracturing. Geophys J Int, 205(3): 1859–1873

Laubach S E (2003). Practical approaches to identifying sealed and open fractures. AAPG Bull, 87(4): 561–579

Laubach S E, Olson J E, Gale J F W (2004). Are open fractures necessarily aligned with maximum horizontal stress? Earth Planet Sci Lett, 222(1): 191–195

Liu H L, Zhang J H, Ji Y B, Li X B (2022). The controlling effect of kerogen type of shale on asphaltene nanopore and its exploration significance. Unconventional oil Gas, 9(3): 1–10

Liu H, Sang S, Xue J, Wang G, Xu H, Ren B, Liu C, Liu S (2016). Characteristics of an *in-situ* stress field and its control on coal fractures and coal permeability in the Gucheng block, southern Qinshui Basin, China. J Nat Gas Sci Eng, 36: 1130–1139

Mlella M, Surpless B, Beasley C, Stewart M K, Yazbeck L, De La Rocha L (2014). The effects of weathering on outcrop-based fracture characterization: a case study from the Stillwell Anticline, West Texas. GSA Abstracts with Programs, 46(1): 12

Mullen M J, Pitcher J L, Hinz D, Everts M, Dunbar D, Carlstrom G M, Brenize G R (2010). Does the presence of natural fractures have an impact on production? A case study from the middle Bakken Dolomite, North Dakota. In: Society of Petroleum Engineers

Nie H K, He Z L, Wang R Y, Zhang G R, Chen Q, Li D H, Lu Z Y, Sun C X (2020). Temperature and origin of fluid inclusions in shale veins of Wufeng–Longmaxi Formations, Sichuan Basin, south China: implications for shale gas preservation and enrichment. J

Petrol Sci Eng, 193: 107329

Olson J E, Laubach S E, Lander R H (2007). Combining diagenesis and mechanics to quantity fracture aperture distributions and fracture pattern permeability. Spec Publ Geol Soc Lond, 270(1): 101–116

Paul S, Chatterjee R (2011a). Mapping of cleats and fractures as an indicator of *in-situ* stress orientation, Jharia Coalfield, India. Int J Coal Geol, 88(2–3): 113–122

Paul S, Chatterjee R (2011b). Determination of *in-situ* stress direction from cleat orientation mapping for coal bed methane exploration in south-eastern part of Jharia coalfield, India. Int J Coal Geol, 87(2): 87–96

Pommer L, Gale J F W, Eichhubl P, Fall A, Laubach S E (2012). Using structural diagenesis to infer the timing of natural fractures in the Marcellus shale. In: Unconventional Resources Technology Conference

Qiu Z, Liu B, Dong D, Lu B, Yawar Z, Chen Z, Schieber J (2020). Silica diagenesis in the Lower Paleozoic Wufeng and Longmaxi Formations in the Sichuan Basin, South China: implications for reservoir properties and paleoproductivity. Mar Pet Geol, 121: 104594

Ranjith P G, Wanniarachchi W, Perera M, Rathnaweera T D (2018). Investigation of the effect of foam flow rate on foam-based hydraulic fracturing of shale reservoir rocks with natural fractures: an experimental study. J Petrol Sci Eng, 169: 518–531

Sang S, Liu W, Shen Z, Ma T (2019). A method for extracting 3d fracture geometries and acquiring their mechanical properties from CT scanning images. J Porous Media, 22(10): 1305–1320

Sun X L, Gomez-Rivas E, Alcalde J, Martín-Martín J D, Ma C F, Muñoz-López D, Cruset D, Cantarero I, Griera A, Travé A (2021). Fracture distribution in a folded fluvial succession: the Puig-reig anticline (south-eastern Pyrenees). Mar Pet Geol, 132: 105169

Tabatabaei M, Dahi Taleghani A, Hooker J N (2021). Debonding of cemented natural fractures during core recovery. J Struct Geol, 144: 104272

Tsang Y W (1984). The effect of tortuosity on fluid flow through a single fracture. Water Resour Res, 20(9): 1209–1215

Walton I, Mclennan J (2013). The role in natural fractures in shale gas production. In: Bunger A P, Mclennan J, Jeffrey R, eds. Effective and Sustainable Hydraulic Fracturing. Intech Open: 327–356

Wang R, Pavlin T, Rosen M S, Mair R W, Cory D G, Walsworth R L (2005). Xenon NMR measurements of permeability and tortuosity in reservoir rocks. Magn Reson Imaging, 23(2): 329–331

Wang Y, Li C H, Hu Y Z, Mao T Q (2017). Laboratory investigation of hydraulic fracture propagation using real-time ultrasonic measurement in shale formations with random natural fractures. Environ Earth Sci, 76(22): 768

Zeeb C, Gomez-Rivas E, Bons P D, Blum P (2013). Evaluation of sampling methods for fracture network characterization using outcrops. AAPG Bull, 97(9): 1545–1566

Zeng L B, Lyu W Y, Li J, Zhu L F, Weng J Q, Yue F, Zu K W (2016). Natural fractures and their influence on shale gas enrichment in Sichuan Basin, China. J Nat Gas Sci Eng, 30: 1–9

Zhang Y S, Zhang J C, Yuan B, Yin S X (2018). *In-situ* stresses controlling hydraulic fracture propagation and fracture breakdown pressure. J Petrol Sci Eng, 164: 164–173

Zhang Y Y, He Z L, Jiang S, Lu S F, Xiao D S, Chen G H, Li Y C (2019). Fracture types in the lower Cambrian shale and their effect on shale gas accumulation, Upper Yangtze. Mar Pet Geol, 99: 282–291

Zhao C J, Li J, Liu G H, Zhang X (2020a). Analysis of well stress with the effect of natural fracture nearby wellbore during hydraulic fracturing in shale gas wells. J Petrol Sci Eng, 188: 106885

Zhao G, Ding W L, Sun Y X, Wang X H, Tian L, Liu J S, Shi S Y, Jiao B C, Cui L (2020b). Fracture development characteristics and controlling factors for reservoirs in the Lower Silurian Longmaxi formation marine shale of the Sangzhi Block, Hunan Province, China. J Petrol Sci Eng, 184: 106470

Zheng S Q, Xie X F, Luo L Y, Jing Y, Tang M, Yang R F, Zhong G R, Wang J, Chen Z Y (2019). Fast and efficient drilling technologies for deep shale gas horizontal wells in the Sichuan Basin: a case study of Well Lu 203. Nat Gas Ind, 39(7): 88–93

Zhu W L, Wong T F (1996). Permeability reduction in a dilating rock: network modeling of damage and tortuosity. Geophys Res Lett, 23(22): 3099–3102

Zou C N, Dong D Z, Wang S J, Li J Z, Li X J, Wang Y M, Li D H, Cheng K M (2010). Geological characteristics and resource potential of shale gas in China. Pet Explor Dev, 37(6): 641–653